Submitted to

International Europhysics Conference on High Energy Physics, EPS2005, July 21, 2005, Lisbon
Abstract: **680**
Parallel Session **Hard QCD**

www-h1.desy.de/h1/www/publications/conf/conf_list.html

Photoproduction of Dijets with High Transverse Momenta at HERA

H1 Collaboration

Abstract

The dijet cross section for photon virtualities $Q^2 < 1\,\mathrm{GeV}^2$ and inelasticities $0.1 < y < 0.9$ is measured with the H1 detector at the ep collider HERA. The data sample comprises data collected during the years 1999 and 2000 with an integrated luminosity of $66.6\ \mathrm{pb}^{-1}$. Jets are defined using the inclusive k_t-algorithm and requiring a minimum transverse momentum of the leading jet of $25\,\mathrm{GeV}$. Longitudinal photon momentum fractions of $0.1 < x_\gamma < 1.0$ and longitudinal proton momentum fractions of $0.05 < x_p < 0.7$ are reached. The data are compared to Monte Carlo event generators based on LO QCD processes with parton showers and fragmentation and NLO QCD parton level calculations. Both yield a good description of the measured cross sections over a wide kinematical range.

1 Introduction

The photoproduction of dijets with high transverse momenta is described within perturbative Quantum Chromodynamics (pQCD) by the hard interaction of real photons with partons inside the proton. The high transverse momenta of jets provide the hard scale to make the perturbative approximation applicable. This allows dijet cross sections to be compared with both leading order (LO) and parton shower Monte Carlo generators and next-to-leading order (NLO) pQCD calculations.

At HERA the largest cross section is due to photoproduction, where the beam electron interacts with the proton via the exchange of a photon at small virtualities $Q^2 \approx 0$. This quasi-real photon then interacts with the proton. Two contributions to the total jet cross section are distinguished: so-called *direct processes* where the photon itself scatters off a quark or gluon in the proton and *resolved processes* where the photon fluctuates into partons and one of them participates in the hard scatter. In the latter case the hadronic structure of the photon is described by associated parton densities.

Measurements of the parton distribution functions (PDFs) of the photon and proton respectively, have been performed in several processes. The quark densities in the photon have been determined at e^+e^- colliders. The parton densities of the proton are mainly determined from DIS experiments. Additional Drell-Yan and pp jet data provide the strongest constraints on the gluon density at high x_p. While the quark densities have rather small uncertainties over a wide range in x_p, the uncertainty of the gluon density at $x_p \approx 0.3$ is about 15% and then increases rapidly for larger x_p reaching a factor of two at $x_p \approx 0.5$. Reducing this uncertainty is of much interest for the physics programs of the Tevatron and LHC.

To test both, the predictions of perturbative calculations and the current PDFs parametrisations, this work investigates dijet production at very small squared four-momentum transfers Q^2 in positron proton interactions using the H1 detector at HERA. The transverse momenta of the jets vary from 25 to 80 GeV. The range of the reconstructed photon momentum fraction is $0.1 < x_\gamma < 1.0$ and unlike the e^+e^- data, the photoproduction of jets is directly sensitive to the gluon density in the photon. In case of the proton the reconstructed momentum fraction is in the range of $0.05 < x_p < 0.7$. The results of this work can be used to further constrain parton density functions at momentum fractions and scales, where currently only few measurements are available. However, a direct extraction of PDFs is not possible from this data alone.

This paper presents an update to a previous publication [1] with twice the statistical precision and an improved understanding of the systematic uncertainties of the measurment. In addition, new measurements are made, which examine cross sections with different jet topologies. The goal of this analysis is to provide the best measurement possible for future inclusion in a combined fit with inclusive deep inelastic scattering (DIS) data from H1 and extraction of PDFs and the strong coupling constant $\alpha_s(M_Z)$ as presented in [2].

2 QCD Models

The PYTHIA [3] Monte Carlo contains LO QCD matrix elements of the relevant hard processes, regulated by a minimum cut-off in transverse momentum. Higher order QCD radiation is represented by parton showers in leading-log approximation. PYTHIA uses the Lund string model for hadronisation. Version 6.1 of PYTHIA was used with the leading order parametrisations CTEQ5L for the proton PDFs and GRV-LO for the photon PDFs and with a 1-loop α_s with $\Lambda_{QCD} = 200\,\mathrm{MeV}$. The kinematic range of the generated events covers $Q^2 < 4\,\mathrm{GeV}^2$ and $0.001 < y < 1.0$. PYTHIA predictions provide a good description of data after scaling them up by a factor of 1.2. This factor is obtained by dividing the measured total dijet cross section by the unscaled prediction of PYTHIA.

The HERWIG [4] Monte Carlo is used to study model dependences and is found to produce similar results to PYTHIA, but requires a scale factor of 1.55.

The NLO dijet cross sections on parton level are obtained using a program by Frixione *et al.* [5] based on the subtraction method [6] for the cancellation of infrared singularities. In the calculation of the NLO cross sections a 2-loop α_s is taken with 5 active quark flavours and value $\alpha_s(M_Z) = 0.118$. A value of $\Lambda_{QCD} = 226\,\mathrm{MeV}$ was chosen as used in the CTEQ proton PDFs. As the main parametrisation CTEQ6M [7] was chosen [1]. For the photon the GRV-HO [9] parametrisation is used as the main setting [2]. The uncertainty from the PDFs in the NLO cross section predictions is calculated using the eigenvectors of the CTEQ6M PDFs. It is found to be generally much smaller than the error from the scale uncertainty, except at large x_p, where it grows to be about twice as big as the scale uncertainty.

The renormalisation scale μ_r and factorisation scale μ_f have been set to the sum of the transverse momenta of the outgoing partons divided by two on an event-by-event basis. A test of the effect of the choice of scale was performed by varying the common scale $\mu = \mu_r = \mu_f$ by a factor of 2 up and down. The uncertainty arising from this procedure was found to vary between a few percent and $\pm 30\%$.

The data are also compared to the NLO calculations after correcting the latter for hadronisation effects. The correction (δ_{had}) is defined as the cross section ratio with jets reconstructed from hadrons and from partons (after the parton shower) but before hadronisation as determined from the Monte Carlo models. HERWIG and PYTHIA produce similar hadronisation correction factors and a mean correction factor is used. The uncertainty in the correction factor is taken as half the difference between HERWIG and PYTHIA. The uncertainty of the hadronisation correction factor is in general smaller than the dominant theory uncertainty, which, depending on the phase space of the measurement, is the scale or PDFs.

3 H1 Detector

The H1 detector is described in detail elsewhere[11]. The detector elements important for this analysis are described below.

[1] To test the dependence of the NLO calculation on the proton PDFs the MRST2001 parameterisation [8] was used and found to produce similar results.

[2] To test the dependence of the cross sections on the photon PDF the AFG-HO parameterisation [10] was used and found to produce similar results.

The Liquid Argon (LAr) and SpaCal calorimeters were used to trigger events, reject non photoproduction events with an identified scattered positron and, together with the central tracking chambers, provides a measurement of the hadronic final state energies from which jets are reconstructed. The central tracking chambers are also used to reconstruct the event vertex.

The LAr calorimeter covers a range in polar angle[3] of $4^\circ < \theta < 153^\circ$ with full acceptance. The jet energy calibration agrees at the 1.5% level with the Monte-Carlo simulation. The angular region $153^\circ < \theta < 177^\circ$ is covered by the SpaCal (a lead scintillating fiber Spaghetti Calorimeter) which has a hadronic energy scale uncertainty of 8%. The central tracking detector consists of two concentric drift chambers and has an angular coverage of $15^\circ < \theta < 165^\circ$. The whole detector is immersed in a 1.15T magnetic field.

The luminosity determination is based on the measurement of the Bethe-Heitler process $ep \rightarrow ep\gamma$, where the positron and photon are detected in calorimeters located downstream of the interaction point in the positron beam direction.

4 Event Selection

The data used in this analysis were taken in the years 1999/2000 where positrons of energy 27.6 GeV were brought to collision with protons of 920 GeV, yielding a centre-of-mass energy of 319 GeV. This sample corresponds to a total integrated luminosity of 66.6 pb^{-1}.

Events are triggered by requiring a combination of sub-triggers, utilising different energy thresholds in the LAr calorimeters with additional vertex and timing conditions. The trigger efficiency is above 98% for the event selection used in this analysis.

The event vertex is required to be reconstructed within 35 cm of the nominal z-vertex. This ensures the event can be properly reconstructed and helps to remove proton beam gas background events. Several topological background finder algorithms are used to remove cosmic muon events. Events with a large missing transverse momentum of more than 20 GeV are rejected, removing charged current and any remaining non-ep background events to below the 1% level.

The main source of background comes from neutral current (NC) DIS events, where the positron has been misidentified as a jet. These events are suppressed by removing events with an identified scattered positron and by requiring $0.1 < y < 0.9$, where y has been reconstructed from the hadronic final state. Additional restrictions on the mass of a jet (< 2 GeV) and, where jets have been reconstructed close to holes between LAr modules, on the jet size (< 0.05) help to reduce the overall DIS background to below 2%. The remaining DIS background is subtracted statistically based on predictions from Monte Carlo.

Jets are reconstructed using the inclusive k_t-cluster algorithm [12]. The p_t-weighted recombination scheme is used in which the jets are considered massless and are ordered in p_t. The jets are found in the laboratory frame and are required to be contained in the LAr calorimeter by the restriction that $-0.5 < \eta_{jet} < 2.75$. Only the two highest p_t jets in the chosen η range

[3]H1 uses a right-handed coordinate system with z axis along the the direction of the outgoing proton beam. The polar angle θ is defined with respect to the z axis and the pseudo-rapidity is given by $\eta = -\ln\tan\theta/2$.

are considered. Asymmetric cuts on the jet's p_t are applied to avoid regions of phase space for which the NLO calculations are not safe. The leading jet is required to have $p_{t,max} > 25\,\mathrm{GeV}$ the other jet must have $p_{t,2} > 15\,\mathrm{GeV}$. After applying these cuts, summarised in table 1, the total number of selected events is about $14,000$.

$Q^2 < 1\,\mathrm{GeV}^2$
$0.1 < y < 0.9$
$p_{t,max} > 25\,\mathrm{GeV}$
$p_{t,2} > 15\,\mathrm{GeV}$
$-0.5 < \eta_{jet} < 2.75$

Table 1: Definition of the phase space of the measured dijet cross section

5 Jet Observables

The dijet cross section is studied as a function of the two scaled longitudinal momenta, x_γ and x_p from the photon and proton side respectively, and as a function of the angular distribution of the jets in their centre-of-mass system, $\cos\theta^*$, where

$$x_\gamma = \frac{1}{2yE_e} \cdot \sum_i^2 p_{t,i} \cdot e^{-\eta_i} \tag{1}$$

$$x_p = \frac{1}{2E_p} \cdot \sum_i^2 p_{t,i} \cdot e^{+\eta_i} \tag{2}$$

$$\cos\theta^* = |\tanh(\eta_1 - \eta_2)/2|\,. \tag{3}$$

Here, E_e and E_p are the energies of the positron and proton beams, respectively, $p_{t,i}$ is the transverse momentum of jet i and η_i its pseudorapidity.

6 Data Correction

The data are corrected for detector effects (acceptance, resolution and efficiencies) obtained from Monte Carlo simulations. The correction factors are calculated from the ratio of the cross sections with jets reconstructed from hadrons (hadron level) and from detector objects (detector level). The correction was done using a bin-by-bin method. The bin sizes used in the cross section measurements are matched to the resolution and generally result in high ($> 60\%$) acceptance[4] and purity[5] (the minimum accepted for any bin is 30%). Both HERWIG and PYTHIA produce similar correction factors and a mean correction factor is used. The uncertainty in the correction factor is taken as half the difference between HERWIG and PYTHIA.

[4]The acceptance is defined as the fraction of events generated in a bin that were reconstructed in that bin after detector effects are taken into account.

[5]The purity is defined as the fraction of events reconstructed in that bin in which they were generated.

7 Systematic Uncertainties

For the jet cross sections the following sources of systematic errors are considered. Also presented are the resulting typical error on the cross section:

- Liquid Argon hadronic energy scale is known to within 1.5%, the resulting uncertainties are typically 10 to 20% (correlated).
- SpaCal hadronic energy scale is known to within 8%, resulting in uncertainties of typically 1% (correlated).
- Monte Carlo reweighting to take into account the imperfect description of the data results in typical errors of 5% (uncorrelated).
- The uncertainty in the correction factor arising from the different models results in a typical error of 2% to 5% (uncorrelated).
- The trigger efficiency uncertainty results in an error of 2% (uncorrelated).
- The uncertainty in the DIS background is taken as 20%. This results in an error of less than 1% (uncorrelated) from the background subtraction.
- An overall normalization error of 1.5% is applied from the uncertainty in the luminosity measurement (correlated).

8 Results

The dijet cross section as function of $\cos\theta^*$ is shown in figure 1. This distribution is sensitive to the dynamics of dijet production, i.e. the matrix element of the hard interaction. Here the measurement is presented separately for $x_\gamma < 0.8$ and $x_\gamma > 0.8$ to enrich the resolved or direct component, respectively. The general shape of this cross section is different from what is to be expected by the matrix elements. This is due to the cut in transverse jet momentum that plays a more important role the closer the jets get to the $\pm z$ direction. In order to reduce this effect, the cross section is also given with an additional cut on the dijet mass of $M_{JJ} > 65$ GeV. Then the shape of the distributions is shifted to the expected form of the QCD matrix elements, revealing the different dominating propagator for direct (quark propagator) and resolved (gluon propagator) events [6]. The measurement of the dijet cross section as function of $\cos\theta^*$ is discribed by the NLO calculation although the data tend to lie below the central prediction.

Figure 2 shows the cross section as function of x_γ in two regions of x_p. For $x_p < 0.1$ the fraction of events induced by gluons from the proton side is estimated to be $\approx 70\%$. It decreases to 15% at the highest x_p reached in this analysis. Thus the two regions roughly distinguish between photon-gluon ($x_p < 0.1$) and photon-quark ($x_p > 0.1$) scattering. Over the

[6]The quark propagator is proportional to $(1 - |\cos\theta^*|)^{-1}$ and the gluon propagator is proportional to $(1 - |\cos\theta^*|)^{-2}$. More exactly, the resolved case its not exclusively driven by gluon propagators, but the gluon propagators are absent in LO direct processes.

entire range in x_γ and in both regions of x_p, NLO and data agree within uncertainties which are slightly larger for low x_p. The leading-order Monte Carlo predictions are similar to the NLO results except for the highest x_γ bin, where they are clearly below, but agree better with the data. There the proton structure is well determined from other processes[7] so that the resulting uncertainty from the proton PDFs is almost a factor of two smaller than for $x_p > 0.1$. But at low x_p the experimental uncertainties as well as the scale uncertainty of the NLO calculations are larger than at high x_p.

The cross section as function of x_p is depicted in figure 3. Here the measurement is divided into two regions of x_γ corresponding to a division into resolved and direct enhanced samples. In both regions the agreement between data and NLO is within 10% at low x_p and thus clearly inside the given uncertainties, which are dominated by the uncertainty of the LAr energy scale which grows from slightly below 10% at low x_p to somewhat above 20% at high x_p. They are larger in the resolved enhanced sample. The two other significant contributions to the total uncertainty are the model uncertainty (5%) in the lowest x_p bin and the statistical uncertainty ($\approx 20\%$) in the highest x_p bin. For the theoretical prediction the scale uncertainty is larger at low compared to high x_p. As expected the PDF uncertainty gets large at high x_p. For $x_p > 0.32$ discrepancies between data and NLO get larger than for low x_p, reaching a 40% difference at highest x_p, which corresponds to 1σ in the direct enhanced case and 1.8σ in the resolved enhanced case. This region is very sensitive to the jet cuts and of course the parametrisation of the proton PDFs.

The cross section as a function of $p_{t,max}$ is presented in figure 4 and for x_p in figure 5. As before, the measurement is divided into two regions of x_γ, corresponding to resolved and direct enhanced samples. In addition, the results are divided into three distinct jet topologies: both jets are in the "backward" direction ($\eta_{1,2} < 1$), both jets are in the "forward" direction ($\eta_{1,2} > 1$), and one jet is in the "forward" ($\eta_i > 1$) and one in the "backward" ($\eta_j < 1$) directions[8]. It can be seen that at high values of $p_{t,max}$ or x_p the scale uncertainty of the NLO prediction is at its smallest, this is most evident in the direct enhanced case. There is a tendency for the NLO prediction to overshoot the data when both jets are in the "forward" direction in the $p_{t,max}$ and x_p distributions.

9 Conclusion

The region of $x_\gamma > 0.8$, where the photon interacts directly with the proton, is an ideal facility to test the proton structure as the photon structure plays no significant role here. Also the experimental uncertainties and the NLO scale uncertainty are smaller in this regime, yielding more stringent constraints on the proton PDFs than in the resolved enhanced sample. Extended studies of the $p_{t,max}$ and x_p cross sections have been made which should allow for a study of the impact of the jet data on PDFs from combined fits of these data with measurements of the proton structure function F_2.

[7]Like the HERA F_2 proton structure function measurements for example.

[8]The summation of the three jet topologies reproduces the equivalent cross section without any selection on jet η.

In the future two improvements in the theory should provide an improved QCD analysis. The computation of higher orders will decrease the uncertainties at low x_p due to smaller scale uncertainties and MC@NLO should enable the model uncertainties of the hadronisation corrections to be reduced.

Acknowledgements

We are grateful to the HERA machine group whose outstanding efforts have made this experiment possible. We thank the engineers and technicians for their work in constructing and maintaining the H1 detector, our funding agencies for financial support, the DESY technical staff for continual assistance and the DESY directorate for support and for the hospitality which they extend to the non DESY members of the collaboration.

References

[1] C. Adloff *et al.* [H1 Collaboration], Eur. Phys. J. C **25** (2002) 13 [hep-ex/0201006].

[2] S. Chekanov *et al.* [ZEUS Collaboration], DESY-05-050, submitted to Eur. Phys. J. C [hep-ph/0503274].

[3] T. Sjöstrand, Comput. Phys. Commun. **82** (1994) 74;
T. Sjöstrand *et al.*, Comput. Phys. Commun. **135** (2001) 238 [hep-ph/0010017].

[4] G. Marchesini *et al.*, Comput. Phys. Commun. **67** (1992) 465;
G. Corcella *et al.*, hep-ph/0201201.

[5] S. Frixione, Nucl. Phys. B **507** (1997) 295 [hep-ph/9706545];
S. Frixione and G. Ridolfi, Nucl. Phys. B **507** (1997) 315 [hep-ph/9707345].

[6] Z. Kunszt and D. E. Soper, Phys. Rev. D **46** (1992) 192.

[7] J. Pumplin *et al.*, JHEP **0207** (2002) 12 [hep-ph/0201195].

[8] A. D. Martin, R. G. Roberts, W. J. Stirling and R. S. Thorne, Eur. Phys. J. C **23** (2002) 73 [hep-ph/0110215].

[9] M. Gluck, E. Reya and A. Vogt, Phys. Rev. D **46** (1992) 1973.

[10] P. Aurenche, J. P. Guillet and M. Fontannaz, Z. Phys. C **64** (1994) 621 [hep-ph/9406382].

[11] I. Abt *et al.* [H1 Collaboration], Nucl. Instrum. Meth. A **386** (1997) 310;
I. Abt *et al.* [H1 Collaboration], Nucl. Instrum. Meth. A **386** (1997) 348.

[12] S. Catani, Yu. L. Dokshitzer, M. H. Seymour and B. R. Webber, Nucl. Phys. B **406** (1993) 187.

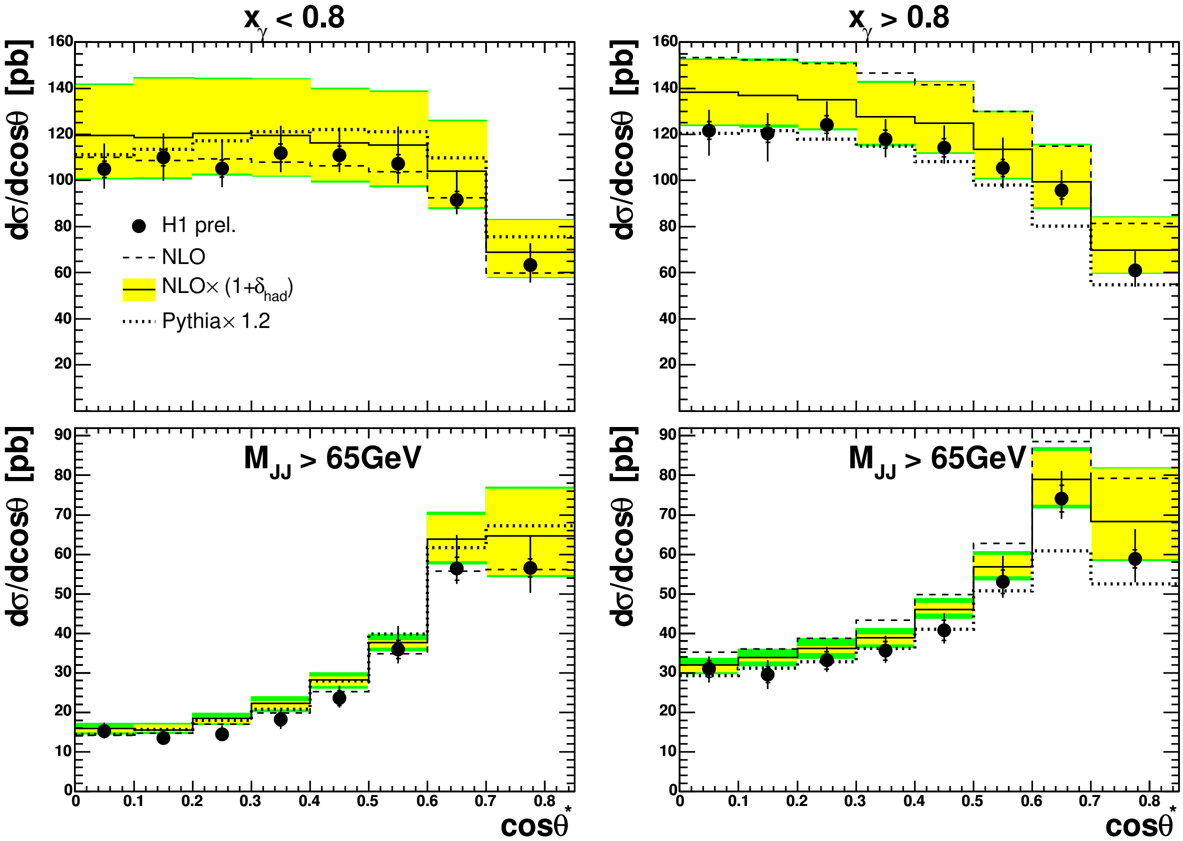

Figure 1: Cross sections in $\cos\theta^*$ for data (points), NLO with (solid line) and without (dashed) hadronisation corrections δ_{had} and for PYTHIA (dotted) scaled by a factor of 1.2. The inner bar of the data points is the statistical, the outer the total uncertainty. The inner band of the NLO$\times(1+\delta_{had})$ result reflects the scale uncertainty, the outer band is the total uncertainty which includes also the one from PDFs and hadronisation. The cross section is shown for two regions in x_γ enhancing the resolved (left) or direct (right) contribution and again with an additional cut on the invariant dijet mass applied.

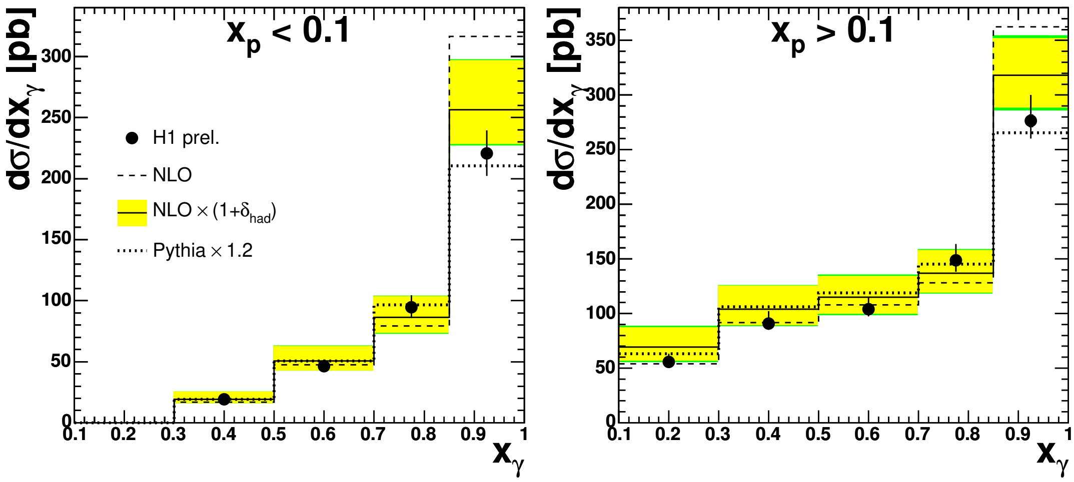

Figure 2: Cross sections in x_γ for data (points), NLO with (solid line) and without (dashed) hadronisation corrections δ_{had} and for PYTHIA (dotted) scaled by a factor of 1.2. The inner bar of the data points is the statistical, the outer the total uncertainty. The inner band of the NLO$\times(1+\delta_{had})$ result reflects the scale uncertainty, the outer band is the total uncertainty which includes also the one from PDFs and hadronisation. The cross section is shown for two regions in x_p.

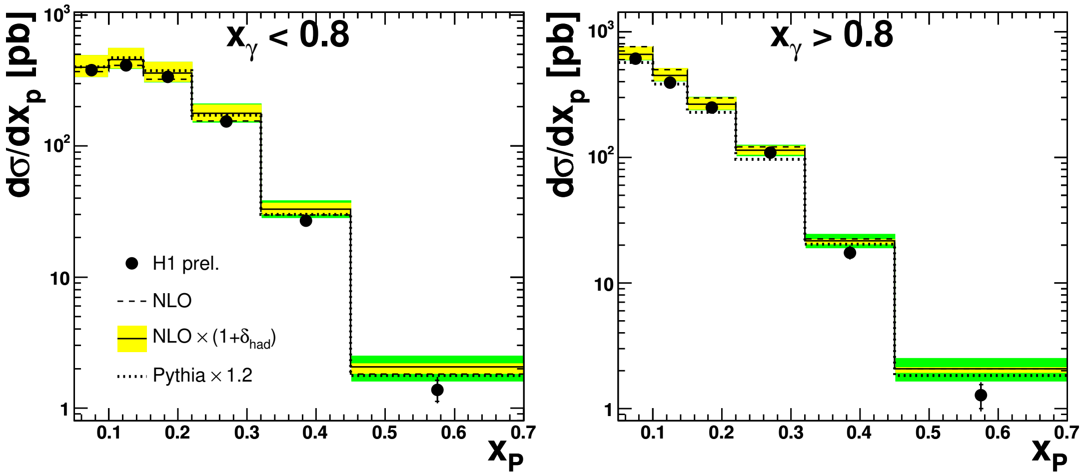

Figure 3: Cross sections in x_p for data (points), NLO with (solid line) and without (dashed) hadronisation corrections δ_{had} and for PYTHIA (dotted) scaled by a factor of 1.2. The inner bar of the data points is the statistical, the outer the total uncertainty. The inner band of the NLO$\times(1+\delta_{had})$ result reflects the scale uncertainty, the outer band is the total uncertainty which includes also the one from PDFs and hadronisation. The cross section is shown for two regions in x_γ enhancing the resolved (left) or direct (right) contribution.

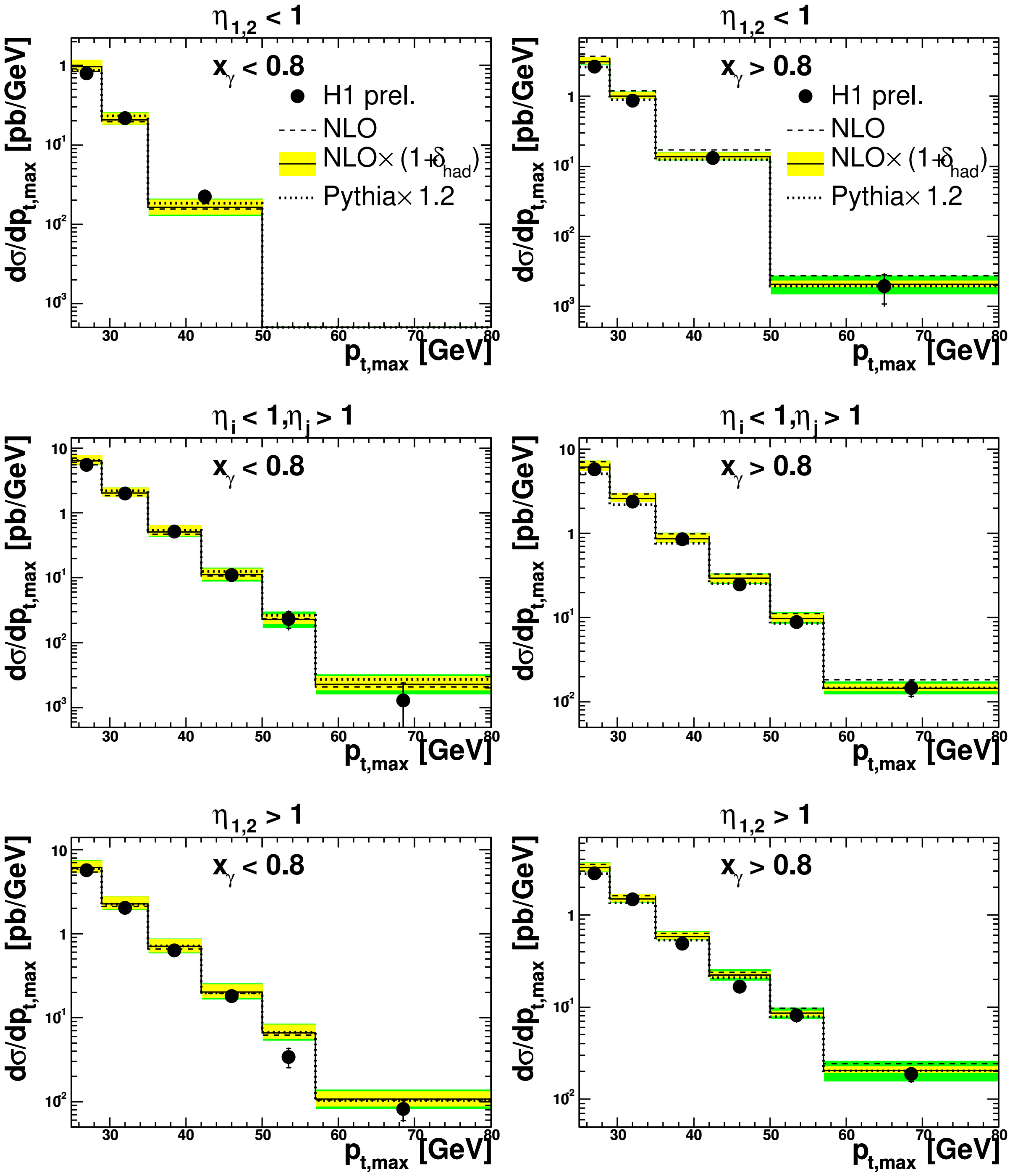

Figure 4: Cross sections in $p_{t,max}$ with different topologies of jet η for data (points), NLO with (solid line) and without (dashed) hadronisation corrections δ_{had} and for PYTHIA (dotted) scaled by a factor of 1.2. The inner bar of the data points is the statistical, the outer the total uncertainty. The inner band of the NLO$\times(1+\delta_{had})$ result reflects the scale uncertainty, the outer band is the total uncertainty which includes also the one from PDFs and hadronisation. The cross section is shown for two regions in x_γ enhancing the resolved (top) or direct (bottom) contribution.

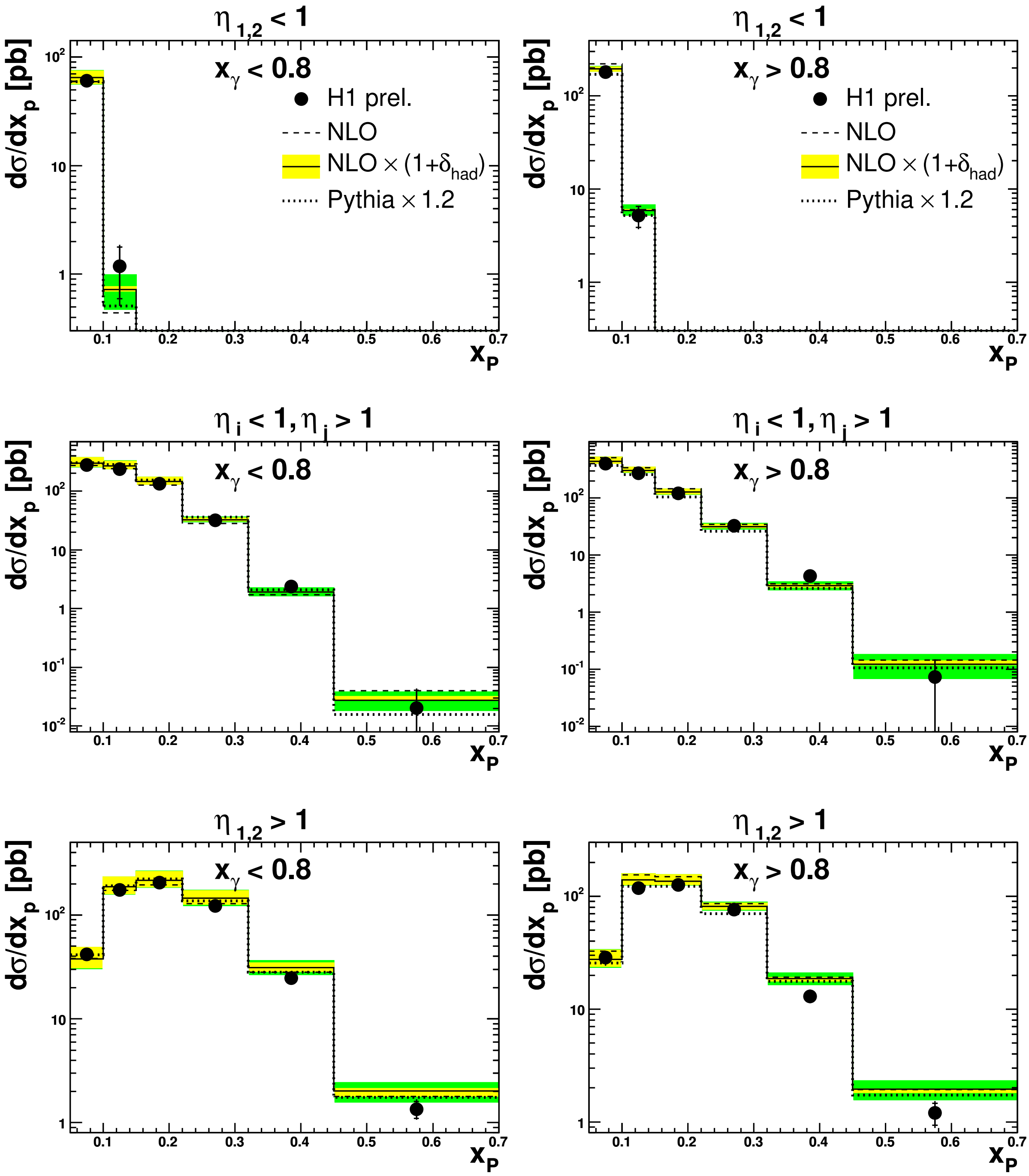

Figure 5: Cross sections in x_p with different topologies of jet η for data (points), NLO with (solid line) and without (dashed) hadronisation corrections δ_{had} and for PYTHIA (dotted) scaled by a factor of 1.2. The inner bar of the data points is the statistical, the outer the total uncertainty. The inner band of the NLO$\times(1+\delta_{had})$ result reflects the scale uncertainty, the outer band is the total uncertainty which includes also the one from PDFs and hadronisation. The cross section is shown for two regions in x_γ enhancing the resolved (top) or direct (bottom) contribution.